HHS Public Access

Author manuscript

J Physiol. Author manuscript; available in PMC 2020 August 01.

Published in final edited form as:

J Physiol. 2019 August ; 597(15): 3867–3883. doi:10.1113/JP278016.

Different paths, same destination: Divergent action potential responses produce conserved cardiac fight-or-flight response in mouse and rabbit hearts

Lianguo Wang[1], **Stefano Morotti**[1], **Srinivas Tapa**[1], **Samantha D. Francis Stuart**[1], **Yanyan Jiang**[1], **Zhen Wang**[1], **Rachel C. Myles**[2], **Kieran E. Brack**[3], **G. André Ng**[3], **Donald M. Bers**[1], **Eleonora Grandi**[1], **Crystal M. Ripplinger**[1]

[1]Department of Pharmacology, School of Medicine, University of California, Davis

[2]Institute of Cardiovascular & Medical Sciences, University of Glasgow, Glasgow, UK

[3]Department of Cardiovascular Sciences, University of Leicester, NIHR Leicester Biomedical Research Centre, Leicester, UK

Abstract

Sympathetic activation of the heart results in positive chronotropy and inotropy, which together rapidly increase cardiac output. The precise mechanisms that produce the electrophysiological and Ca^{2+} handling changes underlying chronotropic and inotropic responses have been studied in detail in isolated cardiac myocytes. However, few studies have examined the dynamic effects of physiological sympathetic nerve activation on cardiac action potentials (AP) and intracellular Ca^{2+} transients (CaT) in the intact heart. Here, we performed bilateral sympathetic nerve stimulation (SNS) in fully innervated, Langendorff-perfused rabbit and mouse hearts. Dual optical mapping with voltage- and Ca^{2+}-sensitive dyes allowed for analysis of spatio-temporal AP and CaT dynamics. The rabbit heart responded to SNS with a monotonic increase in heart rate (HR), monotonic decreases in AP and CaT duration (APD, CaTD), and a monotonic increase in CaT amplitude. The mouse heart had similar HR and CaT responses; however, a pronounced biphasic APD response occurred, with initial prolongation (50.9±5.1ms at t=0sec vs. 60.6±4.1ms at t=15sec, $p<0.05$) followed by shortening (46.5±9.1ms at t=60sec, p=NS vs. t=0). We determined the biphasic APD response in mouse was partly due to dynamic changes in HR during SNS and was exacerbated by β-adrenergic activation. Simulations with species-specific cardiac models revealed that transient APD prolongation in mouse allowed for greater and more rapid CaT responses, suggesting more rapid increases in contractility; conversely, the rabbit heart requires APD shortening to produce optimal inotropic responses. Thus, while the cardiac fight-or-flight

*Corresponding author: Crystal M. Ripplinger, Ph.D., Associate Professor, Department of Pharmacology, UC Davis School of Medicine, 2419B Tupper Hall, One Shields Ave, Davis, CA 95616, Tel: 530-752-1569, Fax: 530-752-7710, cripplinger@ucdavis.edu.

Author contributions

Conception and design of experiments: LW, SM, RCM, KEB, GAN, DMB, EG and CMR; acquisition, analysis and interpretation of data: LW, SM, ST, SDFS, YJ, ZW, EG and CMR; drafting the article or revising it critically for important intellectual content: LW, SM, ST, SDFS, YJ, ZW, RCM, KEB, GAN, DMB, EG and CMR. All experiments were carried out at the University of California, Davis. All authors have read and approved the final version of the manuscript and agree to be accountable for all aspects of the work. All persons designated as authors qualify for authorship, and all those who qualify for authorship are listed.

Competing interests

The authors declare no competing interests.

response is highly conserved between species, the underlying mechanisms orchestrating these effects differ significantly.

Keywords

Optical mapping; sympathetic activation; intracellular Ca^{2+}; action potential; mathematical modelling

Introduction

The fight-or-flight response is a conserved mammalian reaction whereby activation of the sympathetic nervous system is evoked by fear, stress, or exercise (Jansen et al., 1995). In response, key cardiovascular changes occur, including increased cardiac chronotropy, inotropy and lusitropy, which together result in a rapid increase in cardiac output (Bers, 2002). Although these responses are necessary to meet physical demands, the fight-or-flight response may also be associated with electrophysiological abnormalities, triggered activity, and the onset of lethal arrhythmias (Meng et al., 2018), particularly in the setting of underlying cardiovascular disease (Fukuda et al., 2015). Thus, an integrated understanding of the fight-or-flight response is essential for discerning physiological from pathophysiological remodelling, and for optimizing therapies aimed at improving contractile dysfunction and preventing arrhythmias.

The fight-or-flight response is mediated by the sympathetic nervous system and initiated by noradrenaline (NA, primarily released from the cardiac sympathetic nerves) and epinephrine (released from the adrenal medulla) binding to β-adrenergic receptors on cardiomyocytes (Bers, 2002). Mechanistic studies of the fight-or-flight response often involve application of β-adrenergic agonists, e.g., isoproterenol, to isolated myocytes or hearts. Unfortunately, these non-physiological approaches do not fully replicate the heterogeneous distribution of the cardiac sympathetic nerve fibres, which may become even more heterogeneously distributed in cardiovascular disease (Gardner et al., 2015). Agonist application is also unable to recapitulate the temporal kinetics of local neurotransmitter release and reuptake. Furthermore, adrenergically-mediated changes in electrophysiology and contraction at the cellular level are often studied independent of simultaneous changes in heart rate (HR), a key aspect of the integrated fight-or-flight response, which may fundamentally alter cellular responses.

Positive chronotropy is mediated by phosphorylation-dependent changes in intracellular Ca^{2+} handling as well as by cAMP-mediated increases in the pacemaker current, also known as the funny current (I_f), which act to accelerate the sinoatrial node coupled membrane and Ca^{2+} clock (DiFrancesco & Tortora, 1991; Lakatta et al., 2010; Vetulli et al., 2018). At the ventricular myocyte level, positive inotropy is primarily mediated by phosphorylation of L-type Ca^{2+} channels (carrying I_{CaL}), phospholamban (PLB), and ryanodine receptors (RyRs), which increase the Ca^{2+} available for contraction. Enhanced Ca^{2+} and PLB phosphorylation also favour faster relaxation (lusitropy). Faster heart rates and phosphorylation of K^+ channels often counter-balance increases in I_{CaL} and allow the action potential (AP) duration

(APD) to shorten, which may be necessary to accommodate shorter cycle lengths (Terrenoire et al., 2005).

The mouse model is a mainstay in cardiovascular research (Camacho et al., 2016), yet systematic investigation of the detailed electrophysiological and Ca^{2+} handling changes that occur in the intact mouse heart in response to physiological sympathetic nerve activity has just begun (Francis Stuart et al., 2018). Moreover, the mouse heart has electrophysiological and Ca^{2+} handling characteristics that differ dramatically from those of larger mammals, yet the fight-or-flight response is highly conserved across species. Therefore, we sought to investigate the electrophysiological and Ca^{2+} handling response to sympathetic nerve stimulation (SNS) in the mouse heart compared to the more human-like rabbit heart (Edwards & Louch, 2017). To do so, an *ex vivo*, fully innervated Langendorff-perfused heart model (Ng et al., 2001) was optically mapped with voltage- and Ca^{2+} sensitive dyes and mechanisms of the cardiovascular fight-or-flight response were determined.

Despite expected increases in HR in both mouse and rabbit hearts, our results indicate that the spatio-temporal response of the ventricular AP to sympathetic nerve activity was significantly different between species, although intracellular Ca^{2+} signals were similarly enhanced. Interestingly, mathematical modelling revealed that these divergent AP responses actually allow for more robust increases in intracellular Ca^{2+}, and had the AP not responded differently between species, suboptimal increases in inotropy and lusitropy would occur. Thus, while the fight-or-flight response is highly conserved among vertebrates, the mechanisms by which target organ responses are orchestrated may differ significantly across species.

Methods

Ethical approval

All procedures involving animals were approved by the Animal Care and Use Committee of the University of California, Davis (Reference No. 20991), and adhered to the Guide for the Care and Use of Laboratory Animals published by the National Institutes of Health (NIH Publication N0. 85-23, revised 2011). The authors have read, and the experiments comply with, the polices and regulations of *The Journal of Physiology* given by Grundy (Grundy, 2015). Male wild-type C57BL/6J mice (12-16 weeks old, n=13; Jackson Laboratory) and male New Zealand White rabbits (3.0 to 3.5 kg, n=9; Charles River Laboratories) were housed on a 12-h light-dark cycle and given access to food and water *ad libitum*.

Innervated whole-heart Langendorff perfusion

Innervated rabbit hearts were prepared as described previously (Ng et al., 2001) with modifications. Briefly, the rabbits were euthanized with a single intravenous injection of pentobarbital sodium (>100 mg/kg) with concomitant heparin (1000 IU, Fresenius Kabi USA, IL) and bisected sub-diaphragmatically. The thoracic cavity was opened with incisions on both sides and the anterior portion of the ribcage was removed. The pericardium was cut, and ice-cold Tyrode's solution was applied to the surface of the heart. The descending aorta was cannulated with an 8-gauge cannula. The heart was then flushed with 50 mL ice-cold

cardioplegic solution (composition in mmol/L: NaCl 110, $CaCl_2$ 1.2, KCl 16, $MgCl_2$ 16, and $NaHCO_3$ 10). The pulmonary artery was cut to allow outflow of solution from the right ventricle. The preparation extending from the neck (C1) to thorax (T12) was dissected from surrounding tissues and submerged in ice-cold cardioplegic solution. The preparation was then securely positioned supine in a glass-jacketed perfusion chamber.

Isolated, innervated mouse hearts were prepared using a method described by Paton (Paton, 1996) with modifications (Francis Stuart et al., 2018). Mice were administered an IP injection of heparin (100 IU) and euthanized with pentobarbital sodium (>150 mg/kg, IP) and bisected sub-diaphragmatically. The preparation was submerged in ice-cold cardioplegic solution (composition in mmol/L: NaCl 110, $CaCl_2$ 1.2, KCl 16, $MgCl_2$ 16, and $NaHCO_3$ 10) and dissected from C1 to T12. The thoracic cavity was opened via incisions on both sides and the anterior portion of the ribcage was removed. The descending aorta was cannulated with a 22-gauge blunt needle. Following cannulation, the pericardium was cut and 5 mL of ice-cold cardioplegic solution was flushed through the preparation to remove blood. The preparation was then positioned supine in a glass-jacketed perfusion chamber.

After transfer of the preparations to the perfusion chamber, the heart and spinal cord were Langendorff-perfused via the descending aorta with oxygenated (95% O_2, 5% CO_2) modified Tyrode's solution of the following composition (in mmol/L): NaCl 128.2, $CaCl_2$ 1.3, KCl 4.7, $MgCl_2$ 1.05, NaH_2PO_4 1.19, $NaHCO_3$ 20 and glucose 11.1 (pH 7.4±0.05). The perfusate was pumped from a reservoir (2L for rabbit; 0.75L for mouse) through an in-line filter and two bubble traps before passing via the cannula to the preparation, and then recirculated from the perfusion chamber back to the reservoir and re-gassed. Major blood vessels from the ribcage were ligated to prevent perfusion leak. Flow rate was adjusted (rabbit heart at ~100 mL/min; mouse heart at ~10 mL/min) to maintain a perfusion pressure of 40-60 mmHg. Two Ag/AgCl disc electrodes were positioned in the bath to record an electrocardiogram (ECG) analogous to a lead I configuration. A customized bipolar pacing electrode was positioned on the left atrial appendage, or the apex of the left ventricular epicardium for cardiac pacing.

Dual optical mapping of transmembrane potential (V_m) and intracellular Ca^{2+}

Dual optical mapping of V_m and intracellular Ca^{2+} was performed as described previously (Myles et al., 2012; Francis Stuart et al., 2018), except the amount of dyes used was doubled due to higher flow rates in the innervated versus traditional Langendorff perfusion. Upon initiation of perfusion, Blebbistatin (Tocris Bioscience; 20 μM), an excitation-contraction uncoupler, was added to the perfusate to reduce energy demand and to eliminate motion artefact during optical recordings. Vecuronium (Cayman Chemical; 5 μM), a non-depolarizing muscle relaxant, was used to eliminate skeletal muscle contraction during SNS (Stalbovskiy et al., 2014; Ashton et al., 2019) in the innervated rabbit heart preparation. Hearts were then loaded with the acetoxymethyl ester form of the fluorescent intracellular Ca^{2+} indicator Rhod-2 (Rhod-2 AM; Invitrogen). For the rabbit heart, 0.5 mL of 2 mg/mL of Rhod-2 AM, for the mouse heart, 0.2 mL of 1 mg/mL of Rhod-2 AM in DMSO containing 10% Pluronic F127 was loaded through an in-line injection port over one minute. Hearts were subsequently stained with the voltage-sensitive dye RH237 (50 μL for the rabbit, and

10 μL for the mouse, of 1 mg/mL in DMSO). The anterior epicardial surface was excited using LED light sources centred at 531 nm and band-pass filtered from 511 to 551 nm (LEX-2; SciMedia). The emitted fluorescence was collected through a THT-macroscope (SciMedia) and split with a dichroic mirror at 630 nm. The longer wavelength moiety, containing the V_m signal, was long-pass filtered at 700 nm and the shorter wavelength moiety, containing the Ca^{2+} signal, was band-pass filtered with a 32 nm filter centred at 590 nm. The emitted fluorescence signals were then recorded using two CMOS cameras (MiCam Ultima-L; SciMedia) with a sampling rate of 1 kHz and 100 × 100 pixels with a field of view of 31×31 mm for the rabbit heart and 10×10 mm for the mouse heart.

Sympathetic nerve stimulation

Sympathetic nerve stimulation (SNS) was performed as previously described (Ng et al., 2001; Francis Stuart et al., 2018). Briefly, an electrophysiology catheter was inserted in the spinal canal at the 12th thoracic vertebra, and the tip was advanced to the level of the second thoracic vertebra to stimulate cardiac sympathetic outflow. A 6F quadripolar catheter (2 mm electrode, 5 mm spacing) for the rabbit, or a 2F octopolar-pacing catheter (0.2 mm electrode, 0.5 mm spacing; CIBer Mouse-EP Catheter; NuMed Inc, Hopkinton, NY) for the mouse, was used for SNS. From previous reports, tolerated stimulation frequencies for SNS in the rabbit are up to 20 Hz and 15 V, without noticeable run-down of the autonomic responses, measured as changes in heart rate and developed pressure (Ng et al., 2001). Therefore, in the present study, SNS was performed at 5-15 Hz and 5-10 V for no more than 60 sec; then the stimulus was turned off to allow heart rate to return to baseline. A single-channel constant-current square-pulse stimulator (Grass Instruments) was used for SNS.

In order to compare the effects of acute β-AR activation, a subset of mouse hearts (n=4) were traditionally Langendorff-perfused as previously described (Gardner et al., 2015) and subjected to acute bolus tyramine infusion (20 μM) to induce release of endogenous NA from sympathetic axons within the heart, or acute infusion of bolus NA (50 nM).

Mathematical modelling and simulation

To explore potential physiological consequences of the different AP responses observed during SNS in rabbit vs mouse, we simulated our models of the rabbit (Bartos et al., 2017) and mouse (Morotti et al., 2014) ventricular myocyte. Both models integrate detailed descriptions of membrane electrophysiology, Ca^{2+} handling (Shannon et al., 2004) and β-adrenergic signalling (Soltis & Saucerman, 2010; Yang & Saucerman, 2012; Morotti et al., 2014; Negroni et al., 2015). Current- and AP-clamp experiments were simulated in the presence of isoproterenol (ISO, 100 nM mimicking maximal activation). In both types of simulations, the pacing rate (an input in our model) was set to replicate the time course of spontaneous HRs measured in experimental preparations. In AP-clamp simulations, the APs used as a voltage command either mimicked the APD time course in experimental recordings or were set constant to the baseline APD. All simulations were performed in MATLAB (The MathWorks, Natick, MA, USA) using the stiff ordinary differential equation solver ode15s. Model codes are available for download at: https://somapp.ucdmc.ucdavis.edu/Pharmacology/bers/, or http://elegrandi.wixsite.com/grandilab/downloads.

Data analysis and statistics

Data analysis was performed using *Optiq* software (Cairn, UK). V_m and Ca^{2+} images were spatially aligned and filtered with a Gaussian spatial filter (radius 3 pixels). For both APs and CaTs, activation time was determined as the time at 50% between baseline and peak amplitude. For APs, repolarization time was determined as the time at 80% return to baseline and action potential duration at 80% (APD_{80}) as repolarization time minus activation time. For CaTs, repolarization (decay) time at 80% was determined as the time at 80% return to baseline and CaT duration at 80% ($CaTD_{80}$) as decay time minus CaT activation time. Unless otherwise indicated, the APD and CaTD data for each heart represent the mean value from the entire mapping field of view. All values are presented as mean±SD. Repeated measures ANOVA or paired t-tests were used to analyse data obtained before and during/after stimulation from the same hearts. A probability value of $P<0.05$ was considered statistically significant.

Results

Integrated HR, AP and CaT responses to sympathetic stimulation

Bilateral SNS was performed in fully innervated Langendorff-perfused rabbit and mouse hearts by inserting an electrophysiology catheter into the spinal canal with the stimulation electrodes at the 1^{st}-3^{rd} thoracic vertebra (5-15 Hz, 7.5 V, up to 60 sec). Both species demonstrated significant increases in HR with SNS (Fig. 1 A and D). APs and intracellular Ca^{2+} transients (CaTs) were optically mapped from the anterior surface of the heart. The rabbit heart showed prototypical responses, including increased frequency, obvious APD and CaT duration (CaTD) shortening (Fig. 1 B and C), and increases in the amplitude of the CaT (when normalized to pre-SNS amplitudes, because the CaT amplitudes ($\Delta[Ca^{2+}]$) are uncalibrated, Fig. 1 B). The mouse heart, however, showed a very different response during SNS. As HR increased (Fig. 1 D), CaT amplitude increased (Fig. 1 E), CaTD shortened, and APD prolonged (Fig. 1 E and F).

When the full time course (60 sec) of SNS was examined, the rabbit heart demonstrated expected responses in which APD and CaTD monotonically decreased as HR monotonically increased (Fig. 2 A and B). In contrast, despite HR monotonically increasing, the mouse heart displayed a marked biphasic APD response, in which APD prolongation first occurred (reaching a maximum at ~15 sec of stimulation) before shortening to near-control values by 60 sec. Despite this biphasic APD response, CaTD monotonically decreased in the mouse, as in rabbit (Fig. 2 D and E). Both species showed similar magnitude and time course of increase in the relative CaT amplitude, suggesting similar inotropic responses (Fig. 2 C and F).

To verify that the biphasic APD response in the mouse was due to β-adrenergic stimulation of the myocardium and not an unintended consequence of electrical nerve stimulation, acute bolus infusion of either tyramine (20 μM, a catecholamine releasing agent) or NE (50 nM) was performed. These acute infusions produced similar APD, CaTD, and HR responses compared to electrical SNS (Fig. 3 A–C). Furthermore, the effects of electrical SNS were completely abrogated by propranolol (10 μM, a β-adrenergic antagonist, Fig. 3D), indicating

that the response was mediated by β-adrenergic receptors. To uncouple changes in HR from β-adrenergic stimulation, a step-wise increase in pacing frequency was used to mimic the HR changes, first without and then with concomitant SNS. Interestingly, increasing the HR without any additional stimulation produced a biphasic APD response, although to a somewhat lesser degree (Fig. 3E, black line). Applying SNS while also performing the step-wise increase in HR acted to prolong APD, further exaggerating the biphasic APD response (Fig. 3E, blue line). On the other hand, if HR was held constant during SNS, the biphasic APD response was eliminated and APD was prolonged compared to baseline (Fig. 3F), although APD in both cases tended to shorten throughout the 60 sec of pacing due to APD accommodation to the pacing rate (Decker & Rudy, 2010; Grandi et al., 2010). Thus, the biphasic APD response during sympathetic stimulation in the mouse is partly due to the dynamic increase in HR and β-adrenergic stimulation further exaggerates it.

Spatio-temporal responses to sympathetic stimulation

We next asked whether the different electrophysiological responses between species impacted the spatio-temporal organization or sequence of activation and repolarization during SNS. When the HR was held constant with atrial pacing, SNS still caused shortening of both APD and CaTD in the rabbit heart, although to a lesser degree (Fig. 4 A and B). The pattern and speed of AP and CaT activation were spatially in-phase and changed little with SNS (Fig. 4 C and D). However, a reversal in the direction of the repolarization wavefront was observed in 8 out of 9 hearts during sympathetic stimulation (Fig. 4E), similar to previous reports in the rabbit heart (Mantravadi et al., 2007). This change in repolarization is due to more substantial APD shortening at the base compared to the apex during SNS (Fig. 4G, Fig 5F), which is consistent with the known gradient in sympathetic innervation in the rabbit heart, in which greater nerve density and abundance of the adrenergically-sensitive slow component of the delayed rectifier potassium current (I_{Ks}) at the base versus apex have been documented (Mantravadi et al., 2007; Ng et al., 2009). Changes to the CaTD during sympathetic stimulation closely resembled the changes in APD (Fig. 4 F and H). Similar changes in repolarization and APD were also observed when HR was allowed to increase with SNS, with a full reversal of repolarization observed by 10 sec of stimulation (Fig. 5).

On the other hand, when HR was controlled with atrial pacing in the mouse heart, SNS caused a prolongation of APD and a shortening of CaTD at 20 sec of SNS (Fig. 6 A and B). Similar to the rabbit, the mouse heart displayed very little change in the sequence or speed of AP and CaT activation during sympathetic stimulation (Fig. 6 C and D). Unlike the rabbit heart, however, the direction of the repolarization wavefront was unaltered in most (7 out of 8) mouse hearts in which repolarization was mapped (Fig. 6E), and the APD prolonged during early SNS (Fig. 6G). Despite the APD prolongation, the CaTD shortened during SNS, which resulted in a CaT decay and CaTD patterns that were spatially distinct from the changes in the AP (Fig. 6 F and H). Further examination of the dynamic changes in repolarization during SNS in the mouse heart revealed that while the HR was increasing, AP activation changed little (Fig. 7 A and B). The repolarization pattern stayed consistent throughout the early stages of SNS, but slightly changed direction in the later stages of stimulation (~40-60 sec) when APD shortening began to occur (Fig. 7 C–E). We did, however, observe a complete reversal of the direction of repolarization in only 1 out of 8

mouse hearts, demonstrating that repolarization can dramatically change in the mouse heart during sympathetic stimulation, but it is likely not the norm.

Implications for the integrated cardiac fight-or-flight response

To assess the physiological implications of the species differences in response to sympathetic stimulation, we turned to mathematical modelling and simulated our models of the rabbit (Bartos et al., 2017) and the mouse (Morotti et al., 2014) ventricular myocyte. Both models integrate detailed descriptions of membrane electrophysiology and dynamical Ca^{2+} (Shannon et al., 2004; Soltis & Saucerman, 2010) and β-adrenergic signalling (Soltis & Saucerman, 2010; Yang & Saucerman, 2012; Morotti et al., 2014; Negroni et al., 2015). Our working hypothesis was that the differential APD response in mouse versus rabbit may be necessary to fine-tune the fight-or-flight response for optimal increases in inotropy and lusitropy in each species. To test this, we performed AP-clamp simulations where the voltage command was a train of rabbit or mouse APs that mimicked the experimentally recorded dynamic changes in heart rate and APD in each species (Fig. 8 A–D, red and black lines). The simulation outputs were the changes in the CaT amplitude (ΔCaT) and time constant of CaT decay (τ), reflective of changes in inotropy and lusitropy, respectively. β-adrenergic activation was applied throughout the entire AP-clamp simulation (100 nM isoproterenol). To determine the impact of species-specific APD changes during sympathetic activity, these outputs were compared to matched AP-clamp simulations in which the APD was either held constant for both species (Fig 8 C–D, blue lines), or the species-specific APD changes were swapped (i.e., transient APD prolongation was simulated in rabbit and monotonic APD shortening was simulated in mouse, Fig 8 C–D, grey lines). In all cases, we simulated the species-specific increases in heart rate according to experimental findings (Fig. 8 A–B, red lines), and the onset of β-adrenergic stimulation at time 0.

In the rabbit, APD shortening increased steady-state enhancement in CaT amplitude compared to the simulations in which APD was either held constant or transiently prolonged (Fig. 8E, black vs. blue and grey lines). APD shortening also hastened early CaT decay compared to both simulations, whereas steady-state CaT decay was similar between simulations of APD shortening and transient APD prolongation (Fig. 8 G, black vs. blue and grey lines). In the mouse, simulating the experimentally-observed transient APD prolongation enhanced the early CaT increase and rate of decay (Fig. 8 F and H, black vs. blue line), whereas the steady-state response was comparable to that predicted when APD was held constant (as the APD is back to its initial value). Monotonic APD shortening, on the other hand, produced a dramatically blunted CaT amplitude response and slower early and steady-state CaT decay (Fig 8 F and H, black vs. grey lines). These intriguing results suggest that species differences in electrophysiological responses to sympathetic activity may allow for more robust increases in intracellular Ca^{2+} and faster decay; thus, enhanced inotropy and lusitropy, respectively, during the fight-or-flight response.

To assess mechanisms governing enhanced Ca^{2+} handling in each species, simulation results were further investigated. In rabbit, the shorter APD increased the driving force for I_{CaL} during repolarization, resulting in an increase in total I_{CaL}. Conversely, in mouse, a longer APD produced an increase total I_{CaL} (Fig. 9). In both species, an increase in total I_{CaL}

augmented Ca^{2+}-induced Ca^{2+} release from the sarcoplasmic reticulum (SR), and led to an increase in the CaT amplitude. A larger CaT resulted in an increase in SR Ca^{2+} ATPase (SERCA) activity. Faster repolarization in the rabbit heart also favoured inward NCX, which may additionally contribute to faster relaxation via Ca^{2+} extrusion from the cytosol (Fig. 9). In mouse, the longer APD led to an outward shift in NCX, which also contributed to CaT augmentation.

Discussion

Here we report integrated cardiac electrophysiological and Ca^{2+} handling responses to sympathetic nerve stimulation and demonstrate marked species differences between the mouse heart and the more human-like rabbit heart. Although both species showed robust increases in HR and in the amplitude of the CaT (indicative of positive inotropy) over 60 sec of sympathetic stimulation, significant spatio-temporal differences in AP responses were evident. Notably, the sequence of repolarization in the mouse heart was not dramatically altered, as it is in the rabbit heart during SNS, and the mouse APD displayed a biphasic response (lengthening and then shortening) during the time course of stimulation. These key differences may provide important insights into how the mouse, with its fast heart rate and short APD, achieves robust increases in inotropy and lusitropy during physiological sympathetic activity; however, these differences also need to be appreciated when utilizing mouse models of human cardiovascular disease.

Integrated fight-or-flight response in the innervated heart preparation

Although detailed mechanistic studies of β-adrenergic signalling have been carried out for decades, these studies often apply adrenergic agonists and measure time-dependent or steady-state responses. While mechanistically revealing, it is impossible for agonists to fully reproduce physiological doses and spatio-temporal kinetics of catecholamine release and reuptake at the nerve terminal, which may differentially stimulate myocytes. For example, recent *in vivo* and *in vitro* evidence suggests that intercellular communication between sympathetic nerves and cardiomyocytes occurs in a quasi-synaptic fashion, with locally elevated NA concentrations, and activation of only those β-adrenergic receptors that are in direct contact with nerves (Prando et al., 2018). This quasi-synaptic communication can result in non-uniform PKA activity within a single myocyte (restricted to areas localized at the nerve terminal), and considering the heterogeneity of nerve density throughout the heart, extremely complex spatio-temporal electrophysiological and Ca^{2+} handling responses may occur. This heterogeneity may be even more pronounced under pathological conditions, such as myocardial infarction, that generate extensive sympathetic nerve remodelling (Gardner et al., 2015). Furthermore, sympathetic activation of the heart results in rapid and dynamic increases in HR that are not typically replicated *in vitro*. Thus, the innervated heart preparation used here allows for full, integrated assessment of the complex cardiac fight-or-flight response, while still allowing for detailed mechanistic investigation via optical mapping.

Species Differences

It is well appreciated that mouse hearts have dramatically different ionic currents and Ca^{2+} handling properties compared to larger species (Bartos et al., 2015; Edwards & Louch, 2017; Huang, 2017). Major differences include a lack of I_{Kr} and I_{Ks} in the mouse heart, with repolarizing currents instead primarily carried by I_{to} and I_{Kur}. During the cardiac cycle, maximal SERCA activity is greater and contributes a much larger proportion of total cytosolic Ca^{2+} removal in mouse compared to rabbit (Bers, 2002). SR Ca^{2+} content is also relatively high in mice compared to larger species, which combined with SR Ca^{2+} release refractoriness may sometimes result in a negative force-frequency relationship (though positive force-frequency relationships have also been reported) (Maier et al., 2000). Despite these underlying differences, a robust cardiac fight-or-flight response is necessary for survival and a detailed understanding of how rodents and larger mammals orchestrate this response may lend insight into normal physiological function and pathophysiological remodelling.

We did not specifically address arrhythmia susceptibility in the present study, as our focus was on normal function. However, several previous studies have linked sympathetic activity with increased dispersion of repolarization and an increase in ventricular arrhythmias (Mantravadi et al., 2007; Ajijola et al., 2015; Greer-Short & Poelzing, 2015; Yagishita et al., 2015). Our results indicate that the direction of repolarization and of CaT decay change in the rabbit heart during SNS (Fig. 4). It is therefore interesting to speculate whether sympathetic activity results in altered local stress-strain relationships or a modified sequence of relaxation that may allow for faster or more efficient refilling of the ventricles (Roe et al., 2018). These aspects of electro-mechanical function are beyond the scope of the present study, but remain an intriguing area for future work.

Sympathetic stimulation in the mouse heart, on the other hand, did not normally change the direction of either repolarization or CaT decay, and these two parameters were also not spatially coupled to one another (Fig. 6). It is unclear why the mouse heart does not typically display more prominent directional changes. We and others have reported a base-to-apex gradient of sympathetic innervation in the mouse heart that is similar to larger species (Mantravadi et al., 2007; Francis Stuart et al., 2018), and accordingly, greater APD prolongation was observed at the base versus the apex of the mouse heart (Fig. 7F). It is possible that the absolute magnitude of APD change in the mouse during SNS is simply not large enough to appreciably alter the repolarization sequence.

Whether the APD shortens or prolongs with β-adrenergic activation depends on the resulting balance of depolarizing and repolarizing currents. In larger mammals, adrenergically-mediated increases in I_{Ks} typically counterbalance concurrent increases in I_{CaL} to produce APD shortening, but transient AP prolongation and arrhythmia have been demonstrated when kinetics of I_{Ks} and I_{CaL} responses are altered (Liu et al., 2012; Xie et al., 2013; Xie et al., 2014). APD restitution kinetics in larger mammals also suggest that shorter diastolic intervals (occurring at faster HRs) shorten the APD. Thus, during sympathetic activity, the direct effects of adrenergic stimulation combined with increased HR can produce robust APD shortening, as was observed in rabbit hearts in both experiments (Fig. 2A) and simulations (Fig. 8I) in the present study. Increased ventricular arrhythmias as a result of

sympathetic nerve stimulation has been linked to APD restitution changes (Ng et al., 2007) in the rabbit, which can be spatially heterogeneous due to differential innervation and I_{Ks} abundance (Ng et al., 2009). The mouse heart, on the other hand, lacks I_{Ks}, but adrenergic activation still results in an increase in repolarizing current via effects on I_{Kur}. In the present study, when pacing rate was controlled, sympathetic stimulation resulted in prolongation of the APD relative to baseline conditions (Fig. 3 E and F) as shown previously (Morotti et al., 2014), suggesting that increases in depolarizing currents (namely I_{CaL}) predominated.

A novel finding in the present study was the marked biphasic APD response in mouse during sympathetic activity that occurred when HR was allowed to accelerate during stimulation (Fig. 2D). This biphasic response also occurred without sympathetic stimulation when pacing rate was increased in a manner similar to HR acceleration with SNS, although to a lesser degree (Fig. 3E). This finding suggests that rate-dependent effects may contribute to the biphasic APD response, and this effect is enhanced by concurrent SNS. The mechanisms underlying the transient APD prolongation are likely multi-factorial, and therefore difficult to tease out experimentally.

Our mouse model simulations suggest that I_{CaL}, which exhibits facilitation upon repetitive pulses (Lee, 1987), contributes to the initial rate-dependent APD prolongation phase, and that I_{Kur} may play a role in the subsequent APD shortening. In fact, despite differences in the baseline APD (vs. experiments), when we simulated a stronger PKA effect on I_{Kur} (from a 20% to a 100% enhancement), and a slower time constant of phosphorylation of I_{Kur} (from 10sec to 30sec, similar to the kinetics of I_{Ks}, (Liu et al., 2012)), we observed a biphasic APD response with similar time course to that experimentally recorded (albeit with a lower absolute APD value, Fig. 8J, green line). In addition, we have previously shown that slow (~min) accumulation of Na^+ at increasing heart rates increases the activity of the outward Na^+/K^+ ATP-ase, which may also play a role in the delayed APD shortening observed here (Grandi et al., 2010; Grandi et al., 2011). However, while the increase in heart rate is expected to increase Na^+, PKA phosphorylation of phospholemman and consequent increase in Na^+/K^+ ATP-ase activity will tend to decrease Na^+ levels. The precise mechanisms governing these complex rate-dependent changes are an important area for further study.

Because dynamic acceleration of HR is the most physiologically-relevant response to sympathetic activity *in vivo*, we assessed how these changes in APD interact with intracellular Ca^{2+} during SNS, which may provide a reflection of resulting contractile activity (i.e., positive inotropy). Our AP-clamp simulations indicate that APD shortening in the rabbit allows for a greater increase in the amplitude and a faster decline of the CaT, suggesting enhanced inotropy and lusitropy, respectively, compared to the simulations in which APD was either held constant or transiently prolonged (Fig. 8 E and G). APD prolongation might be expected to increase I_{CaL}, but the model revealed that in rabbit, a shorter APD produces a faster increase in the driving force for I_{CaL} as the membrane potential repolarizes. This results in an increase in total I_{CaL}, which augments Ca^{2+}-induced Ca^{2+} release (CICR) from the SR and leads to a greater increase in the amplitude of the CaT (Fig. 9). A larger CaT results in an increase in SERCA activity, which can hasten relaxation. Furthermore, the faster AP repolarization in the rabbit heart favours inward NCX, which may also support faster relaxation via Ca^{2+} extrusion from the cytosol (Fig. 9).

On the other hand, transient prolongation of APD in the mouse heart produced advantageous Ca^{2+} handling responses compared to the simulations in which APD was either held constant or monotonically shortened. APD prolongation allowed for a larger maximal CaT amplitude and faster instantaneous CaT decline (Fig. 8 F and H). The model revealed that the longer APD in the mouse allowed for increased total I_{CaL}, which enhanced CICR and SR Ca^{2+} content, and these findings are consistent with previous experimental studies in rodents (Sah et al., 2001; Mork et al., 2009). Furthermore, a longer APD in the mouse produces an outward shift in NCX, which also contributes to CaT augmentation. The faster CaT decline in the mouse is in response to the larger amount of Ca^{2+} released (Fig. 9). Following 60 sec of stimulation, the mouse Ca^{2+} handling parameters are similar in the simulations of transient prolongation and constant APD, because the APDs converge to similar values at steady-state. However, the early enhancement in Ca^{2+} handling may be particularly important during the early phase of a sympathetic surge, in which fast escape from a predator may be of paramount importance. Simulating a monotonic APD decrease in a manner similar to the rabbit produced disadvantageous Ca^{2+} handling responses (Fig. 8 F and H). Thus, although the mouse and rabbit have opposite electrophysiological responses to sympathetic stimulation, these differing characteristics allowed for optimal intracellular Ca^{2+} handling responses in each species.

Genetic differences

Different mouse strains show considerable differences in baseline electrophysiologic parameters (Waldeyer et al., 2009). The fact that our mouse model was originally built using much shorter baseline APD data than observed in our mapping experiments might partly explain its inability to fully replicate the biphasic APD response observed experimentally (Fig. 8J) when positive chronotropy along with onset of β-adrenergic stimulation were simulated (in current clamp; note that these SNS-like conditions led to a predicted monotonic decrease in rabbit APD (Fig. 8I) in good agreement with our experimental data). Nevertheless, in AP-clamp simulations, predicted mouse CaT responses matched well with our experimental measurements. While this gives us confidence that our mechanistic working model is plausible, it also suggests that despite variability in electrophysiologic properties, similar CaT and contractile activity are produced in different mouse strains. Indeed, recent measurements of myocyte shortening demonstrated no significant differences in contraction among genetically diverse mouse strains, despite large variations in their underlying ionic currents (Rees et al., 2018). This study and the results presented here highlight that, despite significant differences in electrophysiology, Ca^{2+} responses (and resulting contractile function) are conserved across mouse strains with genetically diverse backgrounds as well as across species.

Limitations

Here, we utilized state-of-the art experimental and modelling frameworks to analyse AP and CaT responses to sympathetic activity focusing on how changes in repolarization may affect the CaT, as a proxy for contraction. However, because AP-clamp was used in simulations and mechanical uncouplers were used to enable optical recordings (Fedorov et al., 2007), the picture is likely even more complex, given important bi-directional coupling between the AP and CaT, AP and contraction, and CaT and contraction. Future studies that close these gaps

are warranted and will likely shed additional light on mechanisms underlying the cardiac fight-or-flight response. Although SNS electrode placement and threshold testing were performed similarly in both species, it is difficult to quantify the absolute degree of sympathetic activity evoked with electrical stimulation. Even with SNS, HRs are lower than what would be expected *in vivo*, which is likely a consequence of the isolated Langendorff preparation. SNS only evokes neuronal responses, and sympathetic humoral responses (i.e., circulating catecholamines) were not considered in the present study, but this is an important area for future work.

Conclusions

Our experiments and simulations suggest that the observed electrophysiological responses to SNS are likely fine-tuned in each species to allow for optimal cardiac fight-or-flight responses and potential survival advantage. This supports the notion, based on recent discoveries on the inheritance of acquired characteristics, that the analysis of physiological function can be important to the mechanisms of evolutionary change (Noble, 2013).

Acknowledgments

Funding

This work was supported by the American Heart Association grants 15SDG24910015 (EG) and 16GRNT30960054 (CMR); the UC Davis School of Medicine Dean's Fellow award (EG); the National Institutes of Health (NIH) Stimulating Peripheral Activity to Relieve Conditions grants 1OT2OD023848-01 and 1OT2OD026580-01 (EG and CMR); the National Heart, Lung, and Blood Institute R01HL131517 and R01HL141214 (EG), R01HL111600 (CMR), and K99HL138160 (SM); the UC Davis Academic Federation Professional Development Award (LW) and British Heart Foundation Programme Grant RG/17/3/32774 (GAN).

References:

Ajijola OA, Howard-Quijano K, Scovotti J, Vaseghi M, Lee C, Mahajan A & Shivkumar K. (2015). Augmentation of cardiac sympathetic tone by percutaneous low-level stellate ganglion stimulation in humans: a feasibility study. Physiol Rep 3.

Ashton JL, Trew ML, LeGrice IJ, Paterson DJ, Paton JF, Gillis AM & Smaill BH. (2019). Shift of Leading Pacemaker Site during Reflex Vagal Stimulation and Altered Electrical Source-to-Sink Balance. The Journal of physiology.

Bartos DC, Grandi E & Ripplinger CM. (2015). Ion Channels in the Heart. Compr Physiol 5, 1423–1464. [PubMed: 26140724]

Bartos DC, Morotti S, Ginsburg KS, Grandi E & Bers DM. (2017). Quantitative analysis of the Ca(2+)-dependent regulation of delayed rectifier K(+) current IKs in rabbit ventricular myocytes. The Journal of physiology 595, 2253–2268. [PubMed: 28008618]

Bers DM. (2002). Cardiac excitation-contraction coupling. Nature 415, 198–205. [PubMed: 11805843]

Camacho P, Fan H, Liu Z & He JQ. (2016). Small mammalian animal models of heart disease. Am J Cardiovasc Dis 6, 70–80. [PubMed: 27679742]

Decker KF & Rudy Y. (2010). Ionic mechanisms of electrophysiological heterogeneity and conduction block in the infarct border zone. American journal of physiology Heart and circulatory physiology 299, H1588–1597. [PubMed: 20709867]

DiFrancesco D & Tortora P. (1991). Direct activation of cardiac pacemaker channels by intracellular cyclic AMP. Nature 351, 145–147. [PubMed: 1709448]

Edwards AG & Louch WE. (2017). Species-Dependent Mechanisms of Cardiac Arrhythmia: A Cellular Focus. Clin Med Insights Cardiol 11, 1179546816686061. [PubMed: 28469490]

Fedorov VV, Lozinsky IT, Sosunov EA, Anyukhovsky EP, Rosen MR, Balke CW & Efimov IR. (2007). Application of blebbistatin as an excitation-contraction uncoupler for electrophysiologic study of rat and rabbit hearts. Heart rhythm : the official journal of the Heart Rhythm Society 4, 619–626.

Francis Stuart SD, Wang L, Woodard WR, Ng GA, Habecker BA & Ripplinger CM. (2018). Age-related changes in cardiac electrophysiology and calcium handling in response to sympathetic nerve stimulation. The Journal of physiology.

Fukuda K, Kanazawa H, Aizawa Y, Ardell JL & Shivkumar K. (2015). Cardiac innervation and sudden cardiac death. Circulation research 116, 2005–2019. [PubMed: 26044253]

Gardner RT, Wang L, Lang BT, Cregg JM, Dunbar CL, Woodward WR, Silver J, Ripplinger CM & Habecker BA. (2015). Targeting protein tyrosine phosphatase sigma after myocardial infarction restores cardiac sympathetic innervation and prevents arrhythmias. Nature communications 6, 6235.

Grandi E, Pandit SV, Voigt N, Workman AJ, Dobrev D, Jalife J & Bers DM. (2011). Human atrial action potential and Ca2+ model: sinus rhythm and chronic atrial fibrillation. Circulation research 109, 1055–1066. [PubMed: 21921263]

Grandi E, Pasqualini FS & Bers DM. (2010). A novel computational model of the human ventricular action potential and Ca transient. Journal of molecular and cellular cardiology 48, 112–121. [PubMed: 19835882]

Greer-Short A & Poelzing S. (2015). Temporal response of ectopic activity in guinea pig ventricular myocardium in response to isoproterenol and acetylcholine. Frontiers in physiology 6, 278. [PubMed: 26539122]

Grundy D (2015). Principles and standards for reporting animal experiments in The Journal of Physiology and Experimental Physiology. The Journal of physiology 593, 2547–2549. [PubMed: 26095019]

Huang CL. (2017). Murine Electrophysiological Models of Cardiac Arrhythmogenesis. Physiol Rev 97, 283–409. [PubMed: 27974512]

Jansen AS, Nguyen XV, Karpitskiy V, Mettenleiter TC & Loewy AD. (1995). Central command neurons of the sympathetic nervous system: basis of the fight-or-flight response. Science 270, 644–646. [PubMed: 7570024]

Lakatta EG, Maltsev VA & Vinogradova TM. (2010). A coupled SYSTEM of intracellular Ca2+ clocks and surface membrane voltage clocks controls the timekeeping mechanism of the heart's pacemaker. Circulation research 106, 659–673. [PubMed: 20203315]

Lee KS. (1987). Potentiation of the calcium-channel currents of internally perfused mammalian heart cells by repetitive depolarization. Proceedings of the National Academy of Sciences of the United States of America 84, 3941–3945. [PubMed: 2438689]

Liu GX, Choi BR, Ziv O, Li W, de Lange E, Qu Z & Koren G. (2012). Differential conditions for early after-depolarizations and triggered activity in cardiomyocytes derived from transgenic LQT1 and LQT2 rabbits. The Journal of physiology 590, 1171–1180. [PubMed: 22183728]

Maier LS, Bers DM & Pieske B. (2000). Differences in Ca(2+)-handling and sarcoplasmic reticulum Ca(2+)-content in isolated rat and rabbit myocardium. Journal of molecular and cellular cardiology 32, 2249–2258. [PubMed: 11113000]

Mantravadi R, Gabris B, Liu T, Choi BR, de Groat WC, Ng GA & Salama G. (2007). Autonomic nerve stimulation reverses ventricular repolarization sequence in rabbit hearts. Circulation research 100, e72–80. [PubMed: 17363699]

Meng L, Shivkumar K & Ajijola O. (2018). Autonomic Regulation and Ventricular Arrhythmias. Curr Treat Options Cardiovasc Med 20, 38. [PubMed: 29627871]

Mork HK, Sjaastad I, Sejersted OM & Louch WE. (2009). Slowing of cardiomyocyte Ca2+ release and contraction during heart failure progression in postinfarction mice. American journal of physiology Heart and circulatory physiology 296, H1069–1079. [PubMed: 19201998]

Morotti S, Edwards AG, McCulloch AD, Bers DM & Grandi E. (2014). A novel computational model of mouse myocyte electrophysiology to assess the synergy between Na+ loading and CaMKII. The Journal of physiology 592, 1181–1197. [PubMed: 24421356]

Myles RC, Wang L, Kang C, Bers DM & Ripplinger CM. (2012). Local beta-Adrenergic Stimulation Overcomes Source-Sink Mismatch to Generate Focal Arrhythmia. Circulation research 110, 1454-+. [PubMed: 22539768]

Negroni JA, Morotti S, Lascano EC, Gomes AV, Grandi E, Puglisi JL & Bers DM. (2015). beta-adrenergic effects on cardiac myofilaments and contraction in an integrated rabbit ventricular myocyte model. Journal of molecular and cellular cardiology 81, 162–175. [PubMed: 25724724]

Ng GA, Brack KE & Coote JH. (2001). Effects of direct sympathetic and vagus nerve stimulation on the physiology of the whole heart--a novel model of isolated Langendorff perfused rabbit heart with intact dual autonomic innervation. Experimental physiology 86, 319–329. [PubMed: 11471534]

Ng GA, Brack KE, Patel VH & Coote JH. (2007). Autonomic modulation of electrical restitution, alternans and ventricular fibrillation initiation in the isolated heart. Cardiovascular research 73, 750–760. [PubMed: 17217937]

Ng GA, Mantravadi R, Walker WH, Ortin WG, Choi BR, de Groat W & Salama G. (2009). Sympathetic nerve stimulation produces spatial heterogeneities of action potential restitution. Heart rhythm : the official journal of the Heart Rhythm Society 6, 696–706.

Noble D (2013). Physiology is rocking the foundations of evolutionary biology. Experimental physiology 98, 1235–1243. [PubMed: 23585325]

Paton JF. (1996). A working heart-brainstem preparation of the mouse. J Neurosci Methods 65, 63–68. [PubMed: 8815310]

Prando V, Da Broi F, Franzoso M, Plazzo AP, Pianca N, Francolini M, Basso C, Kay MW, Zaglia T & Mongillo M. (2018). Dynamics of neuroeffector coupling at cardiac sympathetic synapses. The Journal of physiology 596, 2055–2075. [PubMed: 29524231]

Rees CM, Yang JH, Santolini M, Lusis AJ, Weiss JN & Karma A. (2018). The Ca(2+) transient as a feedback sensor controlling cardiomyocyte ionic conductances in mouse populations. Elife 7.

Roe AT, Ruud M, Espe EK, Manfra O, Longobardi S, Aronsen JM, Norden ES, Husebye T, Kolstad TRS, Cataliotti A, Christensen G, Sejersted OM, Niederer SA, Oystein Andersen G, Sjaastad I & Louch WE. (2018). Regional diastolic dysfunction in post-infarction heart failure: role of local mechanical load and SERCA expression. Cardiovascular research.

Sah R, Ramirez RJ, Kaprielian R & Backx PH. (2001). Alterations in action potential profile enhance excitation-contraction coupling in rat cardiac myocytes. The Journal of physiology 533, 201–214. [PubMed: 11351028]

Shannon TR, Wang F, Puglisi J, Weber C & Bers DM. (2004). A mathematical treatment of integrated Ca dynamics within the ventricular myocyte. Biophysical journal 87, 3351–3371. [PubMed: 15347581]

Soltis AR & Saucerman JJ. (2010). Synergy between CaMKII substrates and beta-adrenergic signaling in regulation of cardiac myocyte Ca(2+) handling. Biophysical journal 99, 2038–2047. [PubMed: 20923637]

Stalbovskiy AO, Briant LJ, Paton JF & Pickering AE. (2014). Mapping the cellular electrophysiology of rat sympathetic preganglionic neurones to their roles in cardiorespiratory reflex integration: a whole cell recording study in situ. The Journal of physiology 592, 2215–2236. [PubMed: 24665100]

Terrenoire C, Clancy CE, Cormier JW, Sampson KJ & Kass RS. (2005). Autonomic control of cardiac action potentials: role of potassium channel kinetics in response to sympathetic stimulation. Circulation research 96, e25–34. [PubMed: 15731462]

Vetulli HM, Elizari MV, Naccarelli GV & Gonzalez MD. (2018). Cardiac automaticity: basic concepts and clinical observations. J Interv Card Electrophysiol 52, 263–270. [PubMed: 30112616]

Waldeyer C, Fabritz L, Fortmueller L, Gerss J, Damke D, Blana A, Laakmann S, Kreienkamp N, Volkery D, Breithardt G & Kirchhof P. (2009). Regional, age-dependent, and genotype-dependent differences in ventricular action potential duration and activation time in 410 Langendorff-perfused mouse hearts. Basic research in cardiology 104, 523–533. [PubMed: 19288151]

Xie Y, Grandi E, Bers DM & Sato D. (2014). How does beta-adrenergic signalling affect the transitions from ventricular tachycardia to ventricular fibrillation? Europace : European pacing, arrhythmias, and cardiac electrophysiology : journal of the working groups on cardiac pacing,

arrhythmias, and cardiac cellular electrophysiology of the European Society of Cardiology 16, 452–457.

Xie Y, Grandi E, Puglisi JL, Sato D & Bers DM. (2013). beta-adrenergic stimulation activates early afterdepolarizations transiently via kinetic mismatch of PKA targets. Journal of molecular and cellular cardiology.

Yagishita D, Chui RW, Yamakawa K, Rajendran PS, Ajijola OA, Nakamura K, So EL, Mahajan A, Shivkumar K & Vaseghi M. (2015). Sympathetic nerve stimulation, not circulating norepinephrine, modulates T-peak to T-end interval by increasing global dispersion of repolarization. Circulation Arrhythmia and electrophysiology 8, 174–185. [PubMed: 25532528]

Yang JH & Saucerman JJ. (2012). Phospholemman is a negative feed-forward regulator of Ca2+ in beta-adrenergic signaling, accelerating beta-adrenergic inotropy. Journal of molecular and cellular cardiology 52, 1048–1055. [PubMed: 22289214]

Key Points

- Cardiac electrophysiology and Ca^{2+} handling change rapidly during the fight-or-flight response to meet physiological demands.
- Despite dramatic differences in cardiac electrophysiology, the cardiac fight-or-flight response is highly conserved across species.
- In this study, we performed physiological sympathetic nerve stimulation (SNS) while optically mapping cardiac action potentials and intracellular Ca^{2+} transients in innervated mouse and rabbit hearts.
- Despite similar heart rate and Ca^{2+} handling responses between mouse and rabbit hearts, we found notable species differences in spatio-temporal repolarization dynamics during SNS.
- Species-specific computational models revealed that these electrophysiological differences allowed for enhanced Ca^{2+} handling (i.e., enhanced inotropy) in each species, suggesting that electrophysiological responses are fine-tuned across species to produce optimal cardiac fight-or-flight responses.

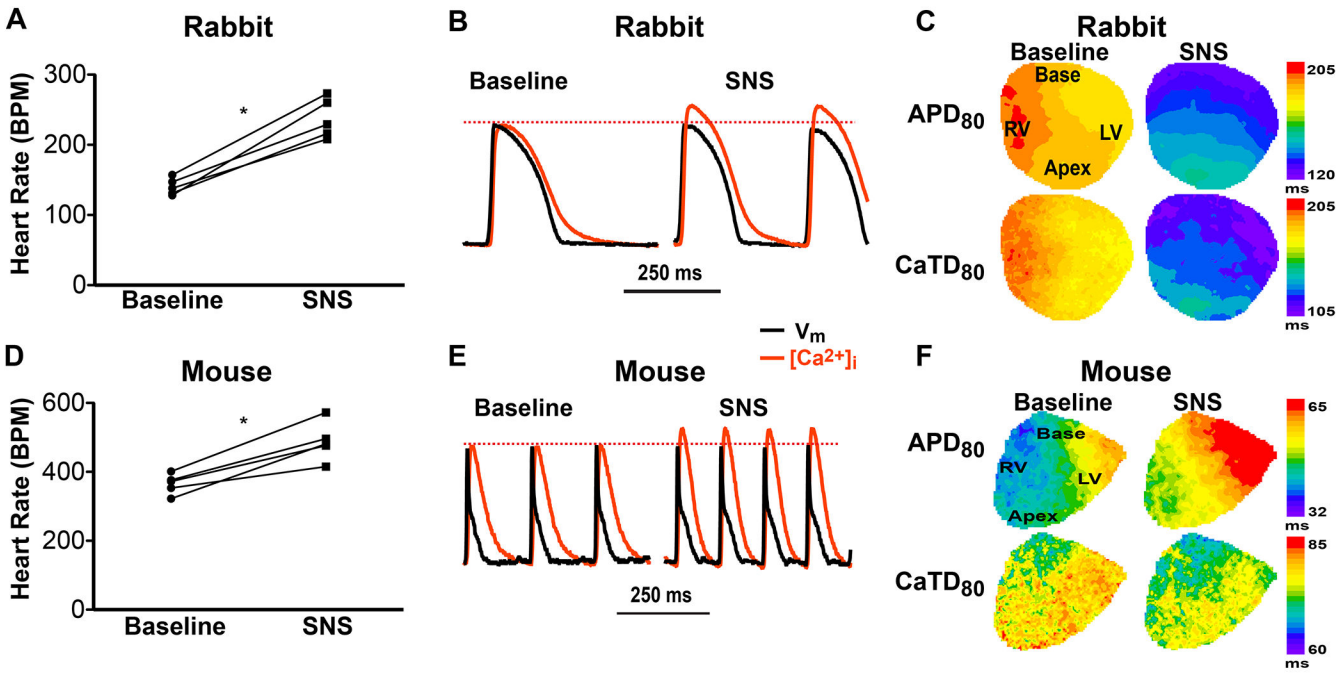

Figure 1.

Effects of sympathetic nerve stimulation (SNS, 20 sec) in innervated isolated rabbit and mouse hearts. *(A)* SNS increased rabbit heart rate (*p<0.05 SNS vs. baseline, n=5). *(B)* Example optical action potentials (APs) and Ca^{2+} transients (CaTs) at baseline and during SNS showing obvious shortening of AP duration (APD), CaT duration (CaTD) and an increase in CaT amplitude (when normalized to baseline amplitude) in the rabbit heart. *(C)* Example maps of APD and CaTD at baseline and during SNS in the rabbit heart. *(D)* SNS increased mouse heart rate (*p<0.05 SNS vs. baseline, n=5). *(E)* Example optical traces as in (B) from a mouse heart. *(F)* Example maps of APD and CaTD at baseline and during SNS in the mouse heart.

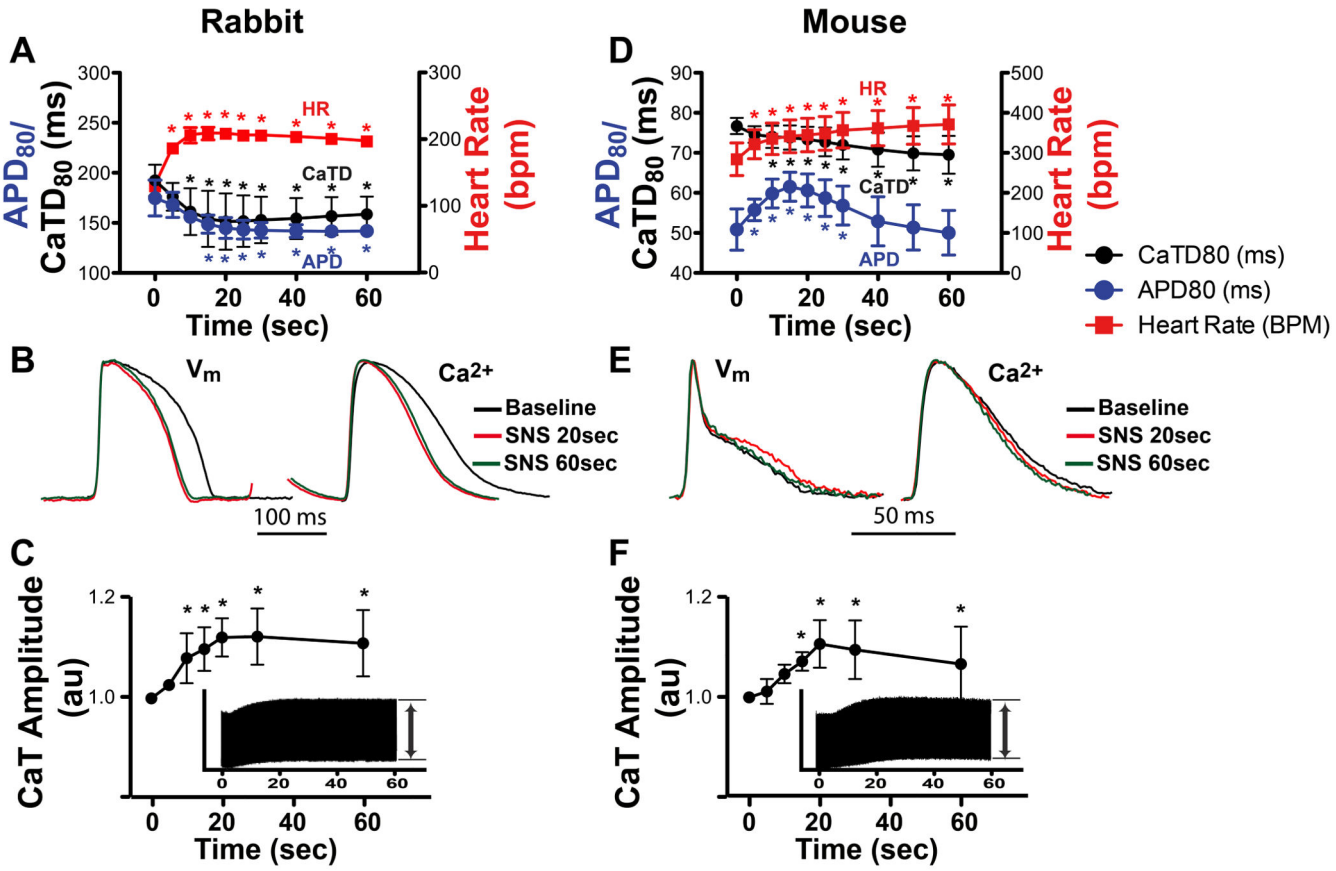

Figure 2.

Effects of sympathetic nerve stimulation (SNS, 60 sec) on heart rate (HR), action potential duration (APD) and Ca^{2+} transients (CaT). *(A)* In rabbit, APD and CaT duration (CaTD) monotonically decreased and HR monotonically increased over 60 sec of stimulation (*p<0.05 vs. time 0, n=4). *(B)* Example optical APs and normalized CaTs at baseline and at 20 and 60 sec of stimulation. *(C)* Relative rabbit CaT amplitude during SNS normalized to baseline (time 0). Inset shows continuous CaT recording over 60 sec from which relative amplitudes were calculated (*p<0.05 vs. time 0, n=6). *(D)* In mouse, HR monotonically increased, CaTD monotonically decreased, and APD displayed a biphasic response (*p<0.05 vs. time 0, n=5). *(E)* Example mouse optical APs and CaTs showing APD prolongation at 20 sec SNS. *(F)* Relative mouse CaT amplitude during SNS (*p<0.05 vs. time 0, n=6).

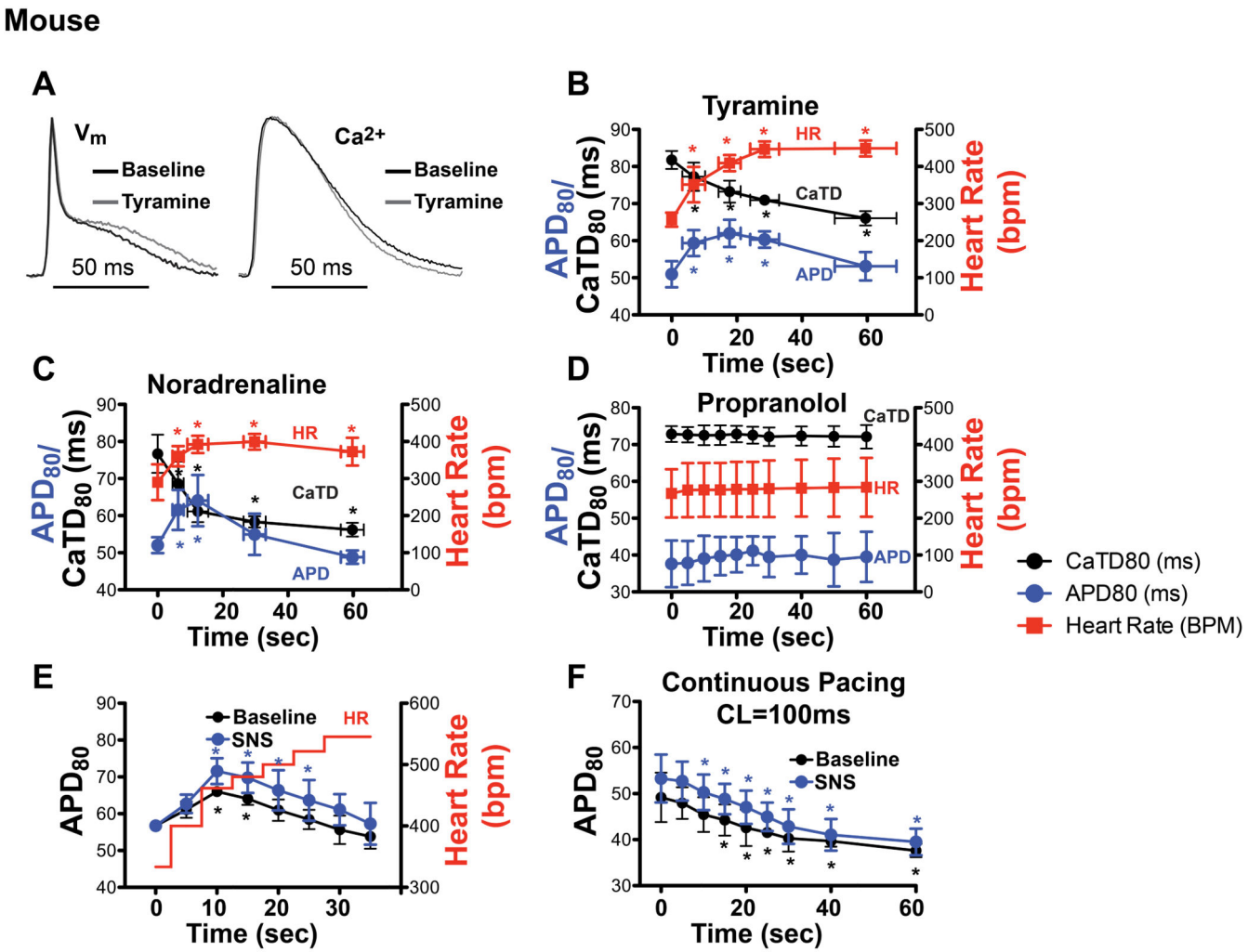

Figure 3.

Impact of β-adrenergic stimulation and heart rate (HR) on action potential duration (APD) and Ca^{2+} transient duration (CaTD) in the mouse heart. *(A)* Example optical APs and normalized CaTs recorded 20 sec after acute tyramine (20 μM) infusion. *(B-C)* HR, APD, and CaTD over 60 sec following acute tyramine (20 μM) bolus infusion (B) or acute noradrenaline (50 nM) bolus infusion (C) (*p<0.05 vs. time 0, n=4). *(D)* HR, APD, and CaTD during 60 sec of sympathetic nerve stimulation (SNS) following pre-treatment with propranolol (10 μM, n=3). *(E)* APD in response to a step-wise increase in pacing frequency (red line), without (black line) and with (blue line) concomitant SNS (*p<0.05 vs. time 0, n=3). *(F)* APD over 60 sec of constant pacing at a cycle length (CL) of 100ms without (black line) and with (blue line) 60 sec of SNS (*p<0.05 vs. time 0, n=5).

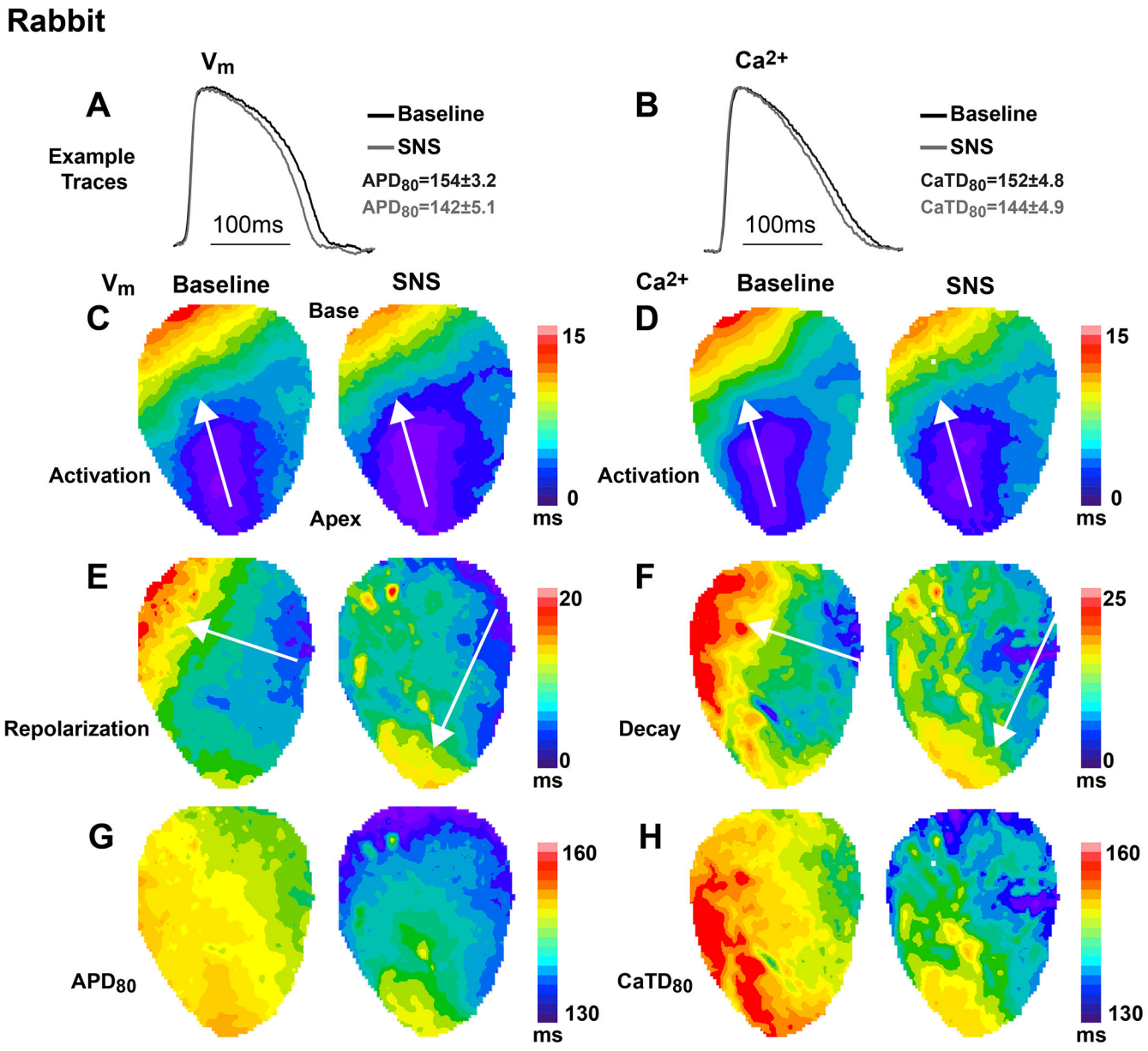

Figure 4.

Spatio-temporal responses to 20 sec of sympathetic nerve stimulation (SNS) in the rabbit heart during constant atrial pacing at a cycle length of 250ms. *(A-B)* Example optical action potentials (APs) and normalized Ca^{2+} transients (CaTs) at baseline (black) and with SNS (grey). Data indicate average change in AP duration (APD) and CaT duration (CaTD) for the heart shown in this figure. *(C-D)* Example maps of AP and CaT activation at baseline and with SNS, which were spatially in-phase and changed little with SNS. *(E-F)* Example maps of repolarization and CaT decay at baseline and with SNS showing a reversal in the direction of the repolarization wavefront with SNS. *(G-H)* Example maps of APD and CaTD illustrating more substantial shortening at the base compared to the apex during SNS.

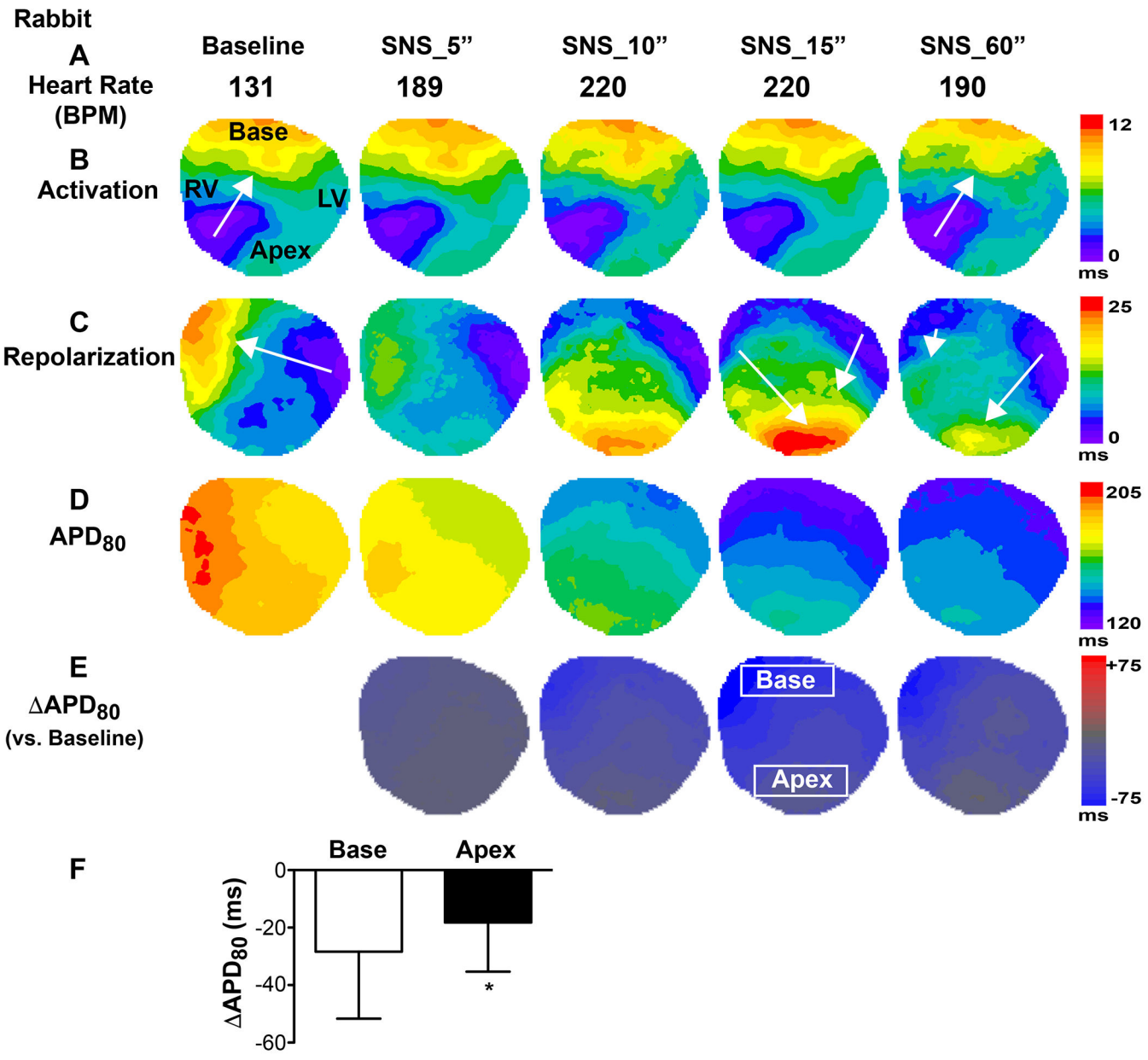

Figure 5.

Spatio-temporal responses to sympathetic nerve stimulation (SNS) in the rabbit heart. *(A)* Heart rate (HR) increased during SNS. *(B)* The pattern and speed of action potential (AP) activation changed little during SNS. *(C)* When HR was allowed to increase during SNS, a full reversal of AP repolarization was observed by 10sec of SNS. *(D-E)* AP duration (APD, D) and change in APD versus baseline (ΔAPD, E) showing the spatio-temporal kinetics of APD shortening. *(F)* Change in APD at 15sec SNS in base and apex regions (regions indicated in E, *p<0.05 base vs. apex, n=4).

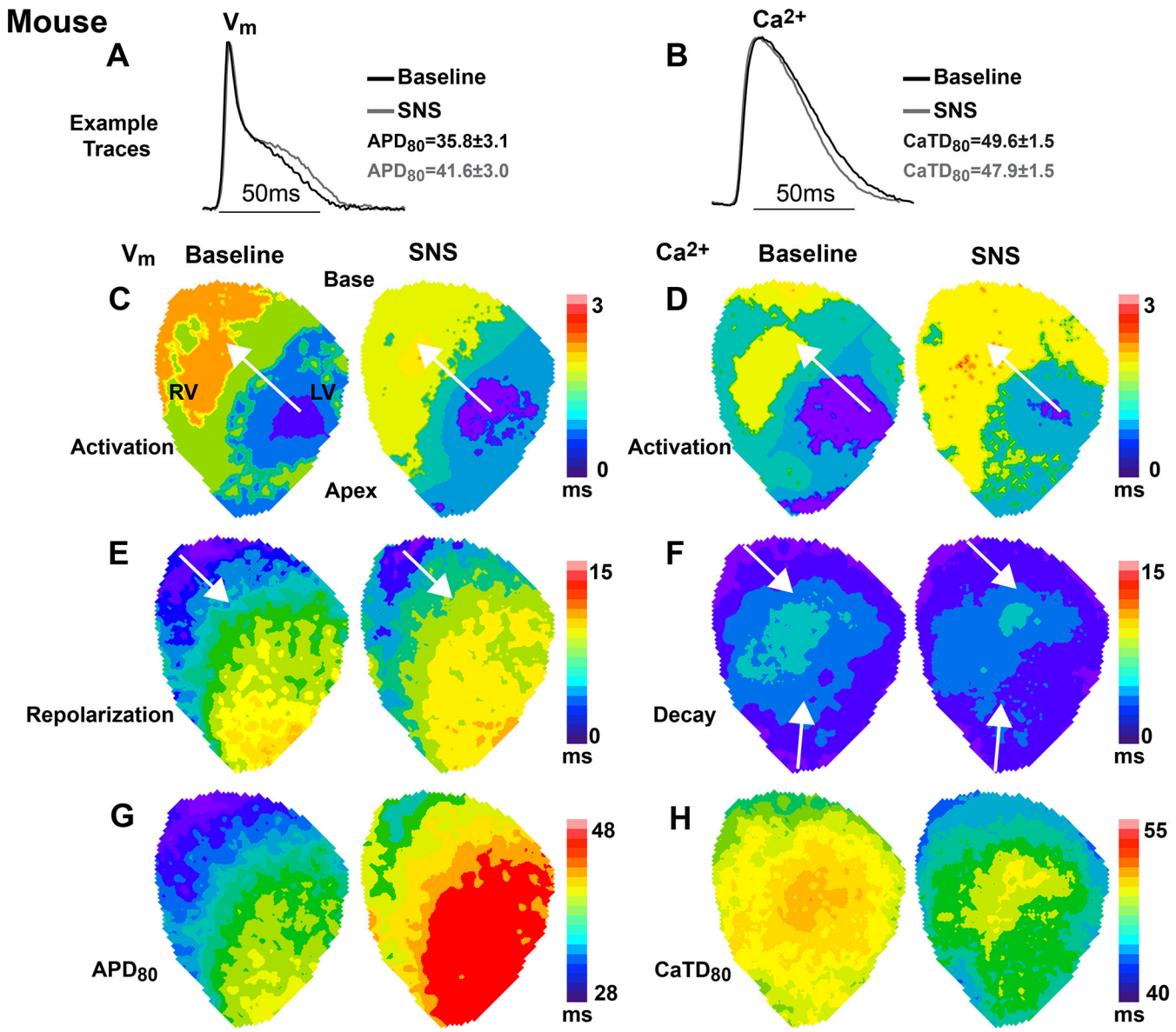

Figure 6.

Spatio-temporal responses to 20 sec of sympathetic nerve stimulation (SNS) in the mouse heart during constant atrial pacing at a cycle length of 100ms. *(A-B)* Example optical action potentials (APs) and normalized Ca^{2+} transients (CaTs) at baseline (black) and with SNS (grey). Data indicate average change in AP duration (APD) and CaT duration (CaTD) for the heart shown in this figure. *(C-D)* Example maps of AP and CaT activation at baseline and with SNS, which were spatially in-phase and changed little with SNS. *(E-F)* Example maps of repolarization and CaT decay at baseline and with SNS showing little change in the direction of repolarization or CaT decay. *(G-H)* Example maps of APD and CaTD showing APD prolongation and CaTD shortening.

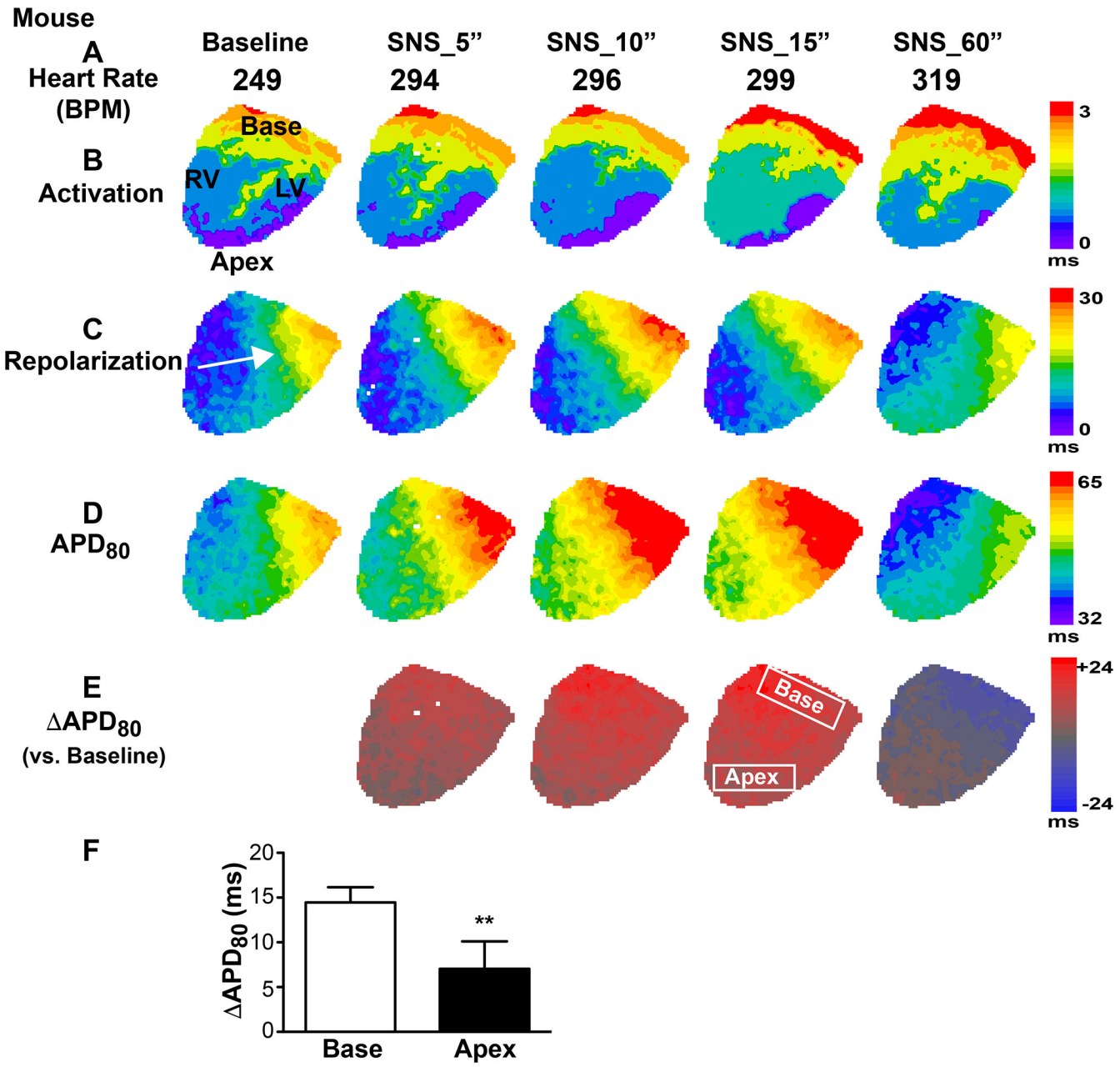

Figure 7.

Spatio-temporal responses to sympathetic nerve stimulation (SNS) in the mouse heart. *(A)* Heart rate (HR) increased during SNS. *(B)* The pattern and speed of action potential (AP) activation changed little during SNS. *(C)* While HR was increasing, the AP repolarization pattern stayed consistent throughout the early stages of SNS, but slightly changed direction in the later stages of stimulation (~40-60 sec) when APD shortening occurred. *(D-E)* AP duration (APD, D) and change in APD versus baseline (ΔAPD, E) showing the spatio-temporal kinetics of APD prolongation followed by shortening. *(F)* Change in APD at 15sec SNS in base and apex regions (regions indicated in E, **p<0.01 base vs. apex, n=5).

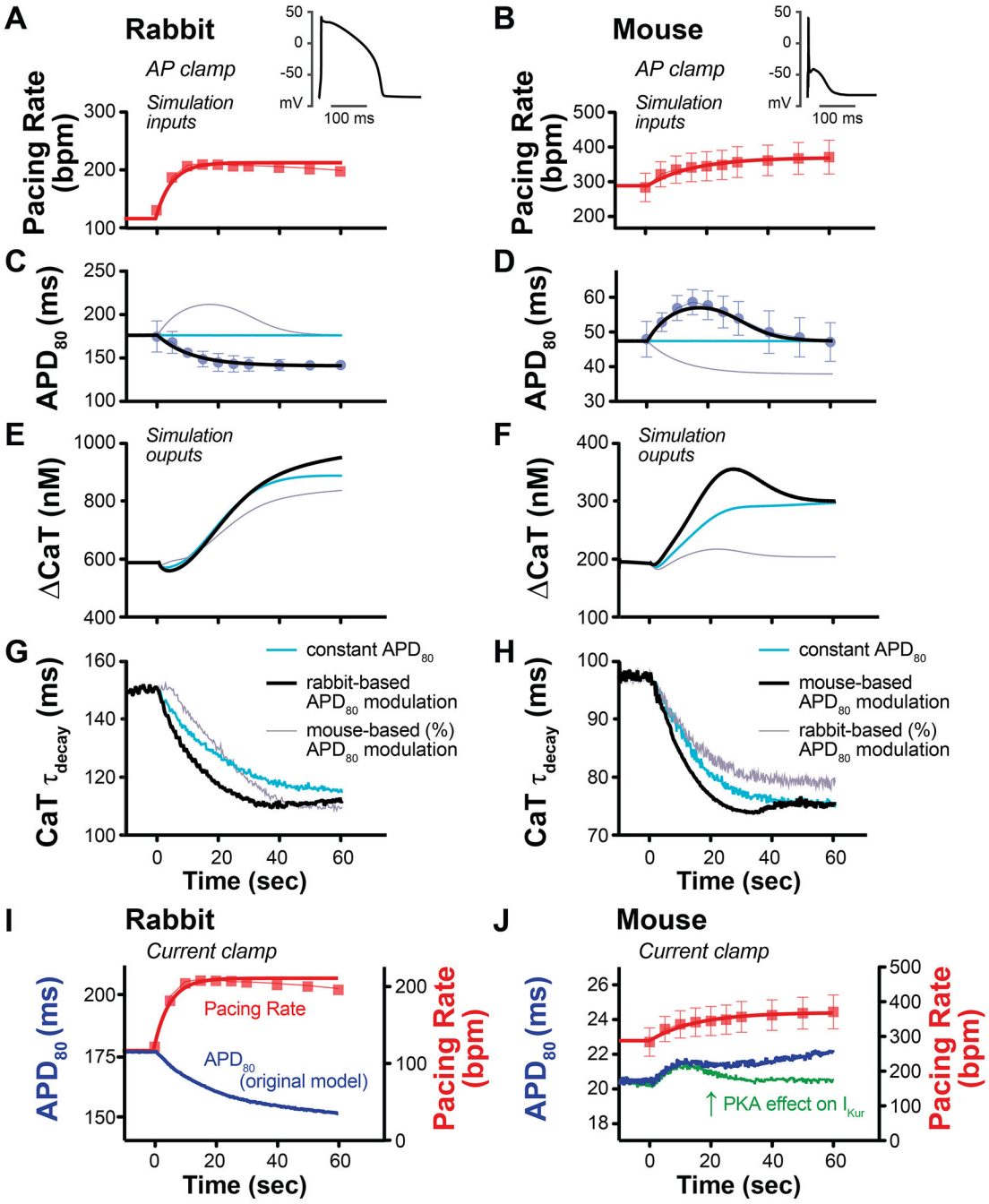

Figure 8.

AP-clamp *(A-H)* and current clamp *(I-J)* simulations with species-specific electrophysiological models. *(A-D)* AP-clamp simulation was performed with a train of rabbit or mouse APs mimicking in rate and duration the experimental responses to sympathetic nerve stimulation (black lines with symbols), a train of constant APDs with increased rate (blue lines), or a train of APDs in which the species-specific responses (APD fractional changes) were swapped (grey lines). In all simulations, rate was increased according to experimental responses (red lines with symbols) and ISO (100 nM) was applied

at time 0. *(E)* In rabbit, APD shortening increased steady-state enhancement in CaT amplitude compared to both constant APD and transiently prolonged APD (black versus blue and grey lines). *(F)* In mouse, transient APD prolongation enhanced the early CaT increase compared to constant APD (peak at approx. 20 sec, black versus blue line) and transient prolongation produced substantial increase in CaT compared to a monotonic decrease in APD (black versus grey line). *(G)* In rabbit, APD shortening hastened early and steady-state CaT decay (CaT τ_{decay}) compared to the simulation in which APD was held constant (black versus blue line), and hastened early CaT decay compared to transient APD prolongation (black versus grey line). *(H)* In mouse, APD prolongation hastened early CaT τ_{decay} compared to constant APD (at approx. 30 sec, black versus blue line). Steady-state responses were comparable (as the APD is back to its initial value). Monotonic APD shortening produced slower early and steady-state CaT decay. *(I)* Current-clamp simulation of SNS-like conditions produced a monotonic decrease in rabbit APD, which was in good agreement with experimental data. *(J)* Current-clamp simulation in mouse produced a slight increase in APD (blue line), but did not fully replicate the biphasic response observed experimentally. When the effect of PKA on I_{Kur} was changed to a 100% increase (from a 20% increase) with a slower phosphorylation time constant (30s vs 10s), a biphasic APD response was elicited (green line).

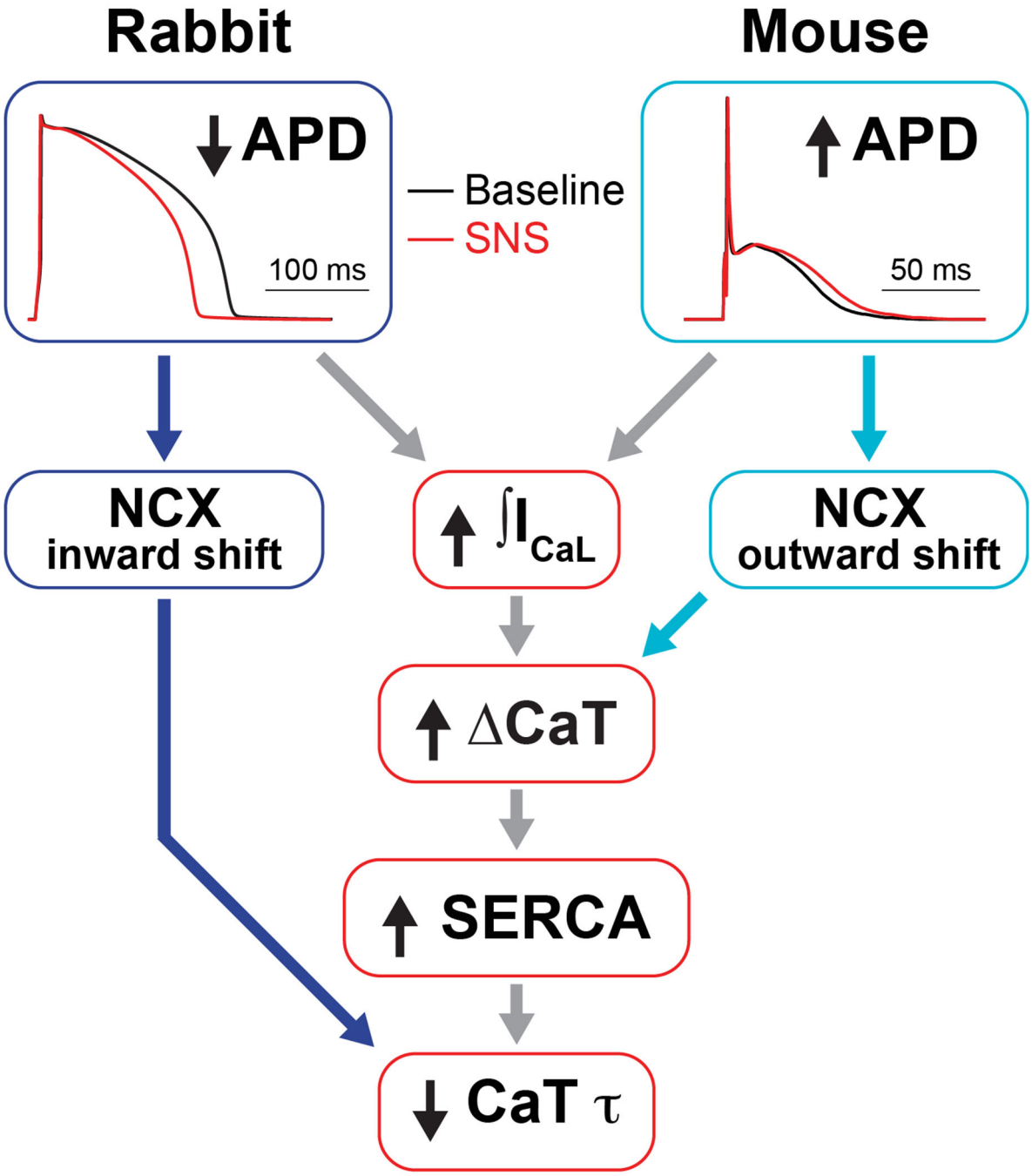

Figure 9.

Interspecies differences in AP repolarization allow for enhancement of inotropy and lusitropy during the fight-or-flight response. Sympathetic stimulation transiently prolongs mouse APD and shortens rabbit APD. In mouse, the longer APD allows for slightly greater Ca^{2+} influx through I_{CaL} and more outward NCX, whereas in rabbit, Ca^{2+} influx is enhanced with shorter APDs due to a faster increase in the driving force for I_{CaL} as the membrane potential falls. Increased Ca^{2+} influx enhances Ca^{2+} transient amplitude (inotropy), which in turn increases SERCA activity that hastens Ca^{2+} transient decay in both

species (lusitropy). Increased inward NCX during the shorter APD also contributes to shorter Ca^{2+} transients in rabbit.